Arch. Metall. Mater. **68** (2023), 1, 137-144

DOI: https://doi.org/10.24425/amm.2023.141487

W. KOWALSKI[1*], H. PAUL[1], I. MANIA[1], P. PETRZAK[1], P. CZAJA[1], R. CHULIST[1], A. GÓRAL[1], M. SZLEZYNGER[1]

# STRUCTURAL CHARACTERIZATION AND PROPERTIES OF Al/Fe MULTI-LAYER COMPOSITES PRODUCED BY HOT PRESSING

This study aimed to develop Fe/Al multilayered metallic/intermetallic composites produced by hot pressing under an air atmosphere. Analyses were carried out on the composite plates made up of alternatively situated sheets of AA1050 aluminum alloy and DN04 low carbon steel, which were annealed at 903 K for 2, 5, and 10 h. Annealing was performed to obtain reaction layers of distinct thickness. The samples were examined using X-Ray diffraction and scanning and transmission electron microscope equipped with an energy-dispersive X-Ray spectrometer. To correlate the structural changes with mechanical properties, microhardness measurements in near-the-interface layers were performed. All the reaction layers grew with parabolic kinetics with η-$Al_5Fe_2$ intermetallic phase as the dominant component. After annealing for 5 and 10 hours, a thin sublayer of θ-$Al_{13}Fe_4$ phase was also detected.

*Keywords:* Fe/Al multilayered composite; intermetallic phase; electron microscopy; microhardness test

## 1. Introduction

Metal-intermetallic layered (MIL) composites based on iron and aluminum are promising materials due to their high specific strength and stiffness at intermediate temperatures and the outstanding corrosion resistance at high temperatures. Such features make them an excellent material especially for the transportation industry [1-5]. Examples of such hybrid designs are lightweight body-in-white structures in transportation systems [6-10], protective aluminum coatings on steel sheets or tubes, motor vehicle exhaust systems, domestic appliances and building cladding panels [11] or heat exchangers in energy conversion systems [12]. Anyway, it is quite difficult to join steel and aluminum using conventional fusion welding methods because of the significantly different melting points (933 K for aluminum and 1420-1768 K for carbon steel, according to the quantity of carbon) and other physico-chemical properties [10]. The use of conventional welding methods leads to the formation of inherently brittle reaction layers in the joint zone. Ongoing research is being carried out to find a solution that allows metallic layers with strongly differing properties to be joined together in the most efficient way. Until now, MIL materials have usually been produced through joining metals, using roll-bonding [13-15], explosive welding [4-8,16], vacuum/gas hot pressing [17-19], friction stir welding [12], or laser welding [20-21]. However, these methods have some disadvantages due to the quality of the joint or the cost of manufacture. For example, in joints obtained by the explosion welding method, strong waviness of the joint surface is observed with a large number of solidified melt regions mainly in the vortexes or on the crests of the wave. The hot-welding technique requires pre-heating of the packets before rolling to reduce the resistance to deformation. This process makes hot-bonding technology expensive and complex. Hot pressing in a gas atmosphere or vacuum requires expensive gas or vacuum plants. Therefore, hot pressing in an atmosphere of air and moderate pressure proves to be an interesting alternative to previously used methods for manufacturing of MIL composites.

The main problem that arises during annealing in an air atmosphere is the oxidation of the materials, therefore a protective atmosphere in the form of inert gas or a vacuum is used. However, this problem can be overcome by applying high pressure which makes it difficult for oxides to appear between the layers. The effectiveness of this method was confirmed during the preparation of Al/Ti composites [22]. During hot pressing, the atoms diffuse from one layer to the other and no oxidation occurs. As proved in [22], the intermetallic layer appeared after

[1] INSTITUTE OF METALLURGY AND MATERIALS SCIENCE, POLISH ACADEMY OF SCIENCES, 25 REYMONTA STR., 30-059 KRAKOW, POLAND

* Corresponding author: w.kowalski@imim.pl

© 2023. The Author(s). This is an open-access article distributed under the terms of the Creative Commons Attribution-NonCommercial License (CC BY-NC 4.0, https://creativecommons.org/licenses/by-nc/4.0/deed.en which permits the use, redistribution of the material in any medium or format, transforming and building upon the material, provided that the article is properly cited, the use is noncommercial, and no modifications or adaptations are made.

1 hour of hot pressing, and the mechanical tests of Al/Ti joints obtained with this method were characterized by high strength and impact strength.

The steel/aluminum MIL composites were previously investigated by many researchers. Kostka et al. [12], investigated friction stir welded joints in plates composed of low carbon-steel/pure aluminum and between joints made of carbon steel/aluminum with a thin sheet of Al-5wt.% Si as intermediate layers. The aluminum/steel interface was characterized on the as-welded samples and samples annealed at temperatures ranging between 473 and 873 K for 9-64 min. For both Al-based alloys, the bonding zone grows with the dominant η-$Al_5Fe_2$ phase after annealing at 723 K and above. The addition of 5wt.% of Si in aluminum alloy results in the formation of ternary $\tau_6$-$Al_{4.5}FeSi$ phase and significantly accelerates the growth of the intermetallic layer. The tensile strength of composites based on pure Al is governed by the Kirkendall porosity at the interface near the reaction layer and the aluminum sheet. Kostka et al. [18], investigated also the formation of intermetallic layers between low-carbon steel and pure Al (99.99%) and between a low-carbon steel and an Al-Si alloy (Al-5 wt.% Si) by solid/solid, solid/semi solid and solid/liquid diffusion at both 873 and 948 K. In both solid/solid and solid/liquid interdiffusion experiments with low-carbon steel and Al, the major dominant was the η-$Al_5Fe_2$ phase. The results shows, that the addition of Si to Al accelerates the reaction with low-carbon steel and finally results with much thicker intermetallic layer as compared to the reaction with pure Al. The formation of ternary Al-Fe-Si phases, designed in the paper as $\tau_1$, $\tau_2$, $\tau_3$, $\tau_5$, $\tau_6$ and $\tau_{10}$ [18]. Springer et al. [19], Yang et al. [20], and Xia et al. [21] reported that the addition of Zn to Al sheet results in the formation of a thick intermetallic layer with η-$Al_5Fe_2$ as a dominant component and a thin layer of the θ-$Al_{13}Fe_4$ phase. The addition of Zn to Al sheet did not result in the formation of ternary phases in the bonding zone, but significantly accelerated the parabolic growth of the intermetallic layer.

A few recent studies have been conducted on aluminum/steel MIL composites obtained by explosive welding [4,5,16]. Loureiro et al. [4], investigated the series of welds to analyze the weldability of stainless steel to aluminum. The results show that the explosive welding was successful only in the case of using stainless steel as a baseplate. Using stainless steel as a flyer plate results in unsuccessful welding due to the very low thermal conductivity of the flyer sheet compared to the baseplate. The welding was always successful when the aluminum alloy sheet was the flyer one. Carbon steel (CS) and aluminum composites obtained by explosive welding were studied by Galvao et al. [5]. In their paper, the structural composition of the interface was analyzed using Kikuchi diffraction in the EBSD technique. Two Al-rich intermetallic phases – $Al_{13}Fe_4$ and $Al_5Fe_2$ were reported in the as-welded state [5]. The structure and the mechanical properties of the stainless steel/Al MIL composites obtained by explosive welding were investigated by Yang et al. [16]. The melted regions contained mainly $Al_{14}Fe_3$ and $Al_5Fe_2$ phases, similar as in [4].

Until now, six intermetallic phases have been identified by previous studies [3-6,9-13,16,18-21] near the Fe/Al interface. The FeAl phase has a simple cubic (B2-type) crystal structure, whereas the Al-rich intermetallic phases $FeAl_2$, $Fe_2Al_5$, and $Fe_4Al_{13}$ (described also as $FeAl_3$ [9]) have more complex structures of the triclinic, orthorhombic, and monoclinic type, respectively [9]. The high temperature of the $Fe_5Al_8$ phase has often been designated in the literature as an ε-phase since their structure was unknown for a long time. This phase decomposes during cooling in a fast eutectoid reaction and cannot be preserved at room temperature [3,9,10,23]. The structure of the $Fe_3Al$ phase from the Fe-rich region of the Al-Fe binary phase diagram was found to be face-centered cubic (Fm3m) [9].

This study aims to thoroughly analyze the interfacial microstructure developed in Al/Fe composite during hot pressing in air. The peculiarities of $Al_nFe_m$ intermetallic formation induced by annealing of such composite under elevated pressure were at the center of interest. The microstructures and chemical composition changes were analyzed using transmission (TEM) and scanning (SEM) electron microscopes equipped with energy dispersive spectrometry (EDS) detectors. Additional XRD diffraction and microhardness measurements for bonding zone were conducted.

## 2. Materials and methods

AA1050 alloy (hereafter denoted as Al) and DC04 low carbon steel (hereafter denoted as Fe) sheets were selected to prepare Al/Fe composite using the hot pressing method. Three composites were made from ten square-shaped Al and eleven Fe sheets, where the Fe sheet was on the top and the bottom of the composites (Fig. 1). The sheet dimensions were 13×13×0.5 $mm^3$ (length×width×thickness). All sheets were ground with abrasive papers of up to 600 grit size, and then cleaned in acetone and rinsed in ethanol to remove the oxides from their surfaces. Then the sheets were stacked in a furnace and pressed with a load of 30 MPa and then annealed at 903 K for 2, 5, and 10 h.

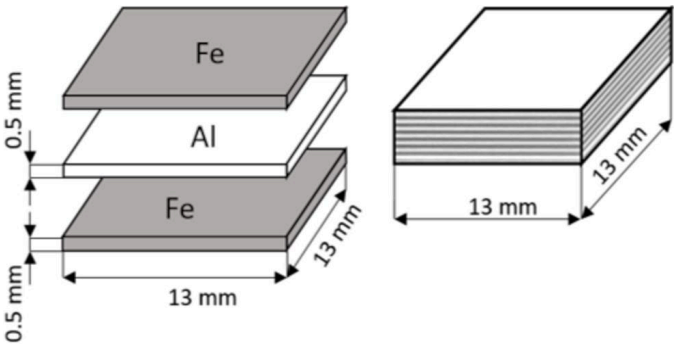


Fig. 1. The scheme for Fe/Al multilayer composite prepared for hot pressing

After hot pressing, the samples were prepared for the microstructure observations. For SEM observations in the backscattered electrons (the SEM/BSE technique) the samples were ground with abrasive papers of grit sizes ranging from 600 to 7000, then polished with a diamond suspension of 3 μm and

1 μm particle sizes. These mesoscale analyses used Philips XL30 SEM operated at 20 kV and equipped with an EDS system for chemical composition analysis.

Nanoscale investigations along the interfaces were conducted using FEI Tecnai G2 200 kV FEG TEM equipped with Fischione High-Angle Annular Dark Field (HAADF) detector for STEM observations and EDAX/EDS spectroscope. For TEM observations, the thin lamellas were obtained using FIB (Focused Ion Beam) technique using FEI Quanta 3D 200 Focused Ion Beam microscope equipped with an Omniprobe lift-out system. Phase analysis was performed using an X-Ray diffractometer (CoKα1 radiation, $\lambda$ = 1.79Å) equipped with a Bragg-Brentano camera. The microstructural observations were supplemented with the microhardness measurements using CSM Instruments microhardness tester. The investigations were performed on polished surfaces of samples annealed for 5 h. The microhardness tests were performed with a Vickers-type indenter and maximum applied load of 1.9614 N. The obtained result was the average of 5 indentations.

## 3. Results and discussion

### 3.1. Microstructural observations

SEM/BSE micrographs show the reaction regions formed between Fe and Al as a result of interdiffusion (Fig. 2). After annealing at 903 K the intermetallic layers (hereafter denoted as Intm.) were formed near all the interfaces for times ranging between 2 h and 10 h. However, a significant increase in the thickness of the intermetallic layer is seen between 2 and 10 h of annealing. The reaction layers are continuous, but their thicknesses vary along the baseline. Regardless of the annealing time, the intermetallic phase grows in the form of finger-like protrusions on the Fe site and is finely serrated toward the Al (Fig. 3a). Such structure was observed earlier by Kostka et al. [18] and Springer et al. [19]. A thin layer at the edge of "the fingers" is observed on SEM/BSE micrographs (Fig. 3b) under all applied annealing times and temperature conditions. Another thin layer was found between the broad intermetallic layer and Al (Fig. 3c). During the growth of the intermetallic layer [12], the formation of structural discontinuities between these layers may be related to the Kirkendall porosity. The volume fraction of pores increases with annealing time. In the central part of the samples annealed for 10 hours, the Al layer completely transforms into an intermetallic phase (Fig. 2c).

The mean layer thickness of the reaction layer is shown in TABLE 1. Based on measurements of the diffusion layers thickness (Fig. 4) the growth kinetic of the intermetallic phase was evaluated. The layer thickness and the annealing time were assessed using the following formula [19]:

$$d = kt^n \tag{1}$$

where: $d$ is the mean layer thickness, $k$ is the growth coefficient, $t$ is the annealing time, and $n$ is the exponential factor.The thickness changes as a function of annealing time showed that

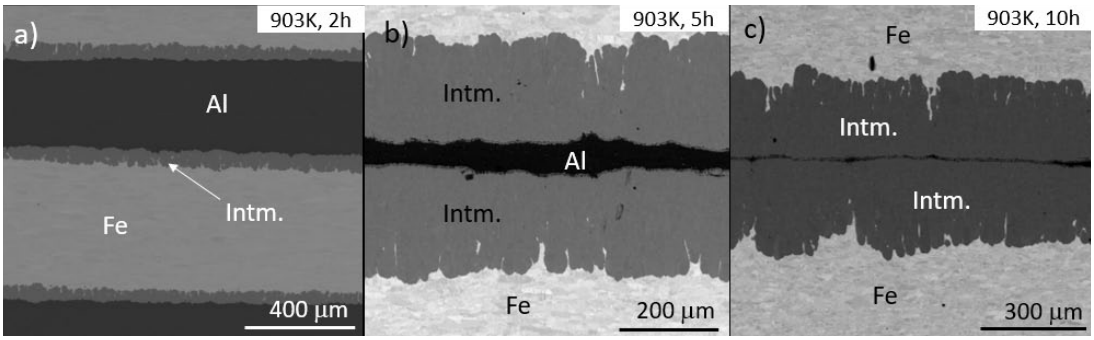


Fig. 2. SEM/BSE images of the bonding zone in Fe/Al MIL composites after hot pressing at different times of annealing. Intm. refers to the intermetallic layer. Images were taken from the central part of the sample (9th interface)

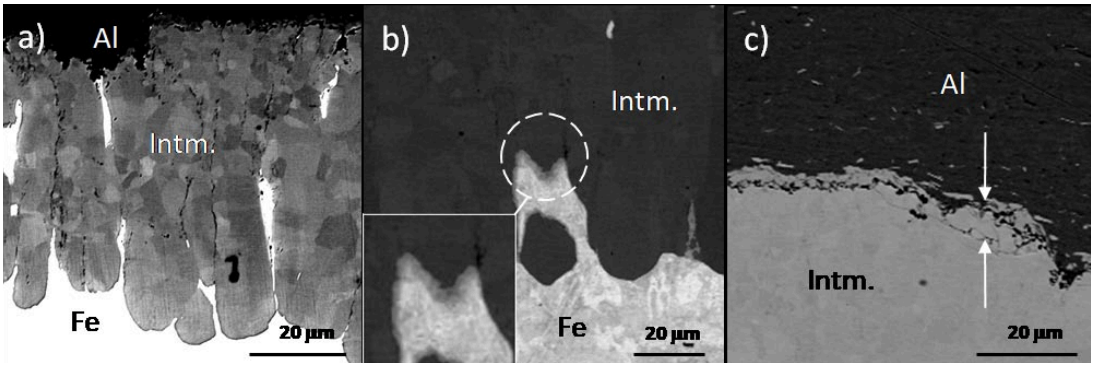


Fig. 3. SEM/BSE observations of the reaction regions between Fe and Al sheets: a) finger-like extrusions of the intermetallic phase in sample annealed at 903 K for 2h; b) the thin layer observed between Fe and Intm. c) the Kirkendall porosity between Intm. and Al

TABLE 1

The average thicknesses ($d$) of intermetallic layers based on the SEM/BSE measurements. The standard deviation is marked as ($\rho$)

| Sample | $T$ [K] | $t$ [h] | $d$ [µm] | $\rho$ [µm] |
|---|---|---|---|---|
| AS-1 | 903 | 2 | 61 | 6 |
| AS-2 | | 5 | 153 | 10 |
| AS-3 | | 10 | 256 | 20 |

the intermetallic layer exhibits parabolic growth kinetics with a growth coefficient of $k = 35.2$ µm/h$^n$ (Fig. 4) and the value of exponential factor of $n = 0.85$. The exponential factor n describes the relationship between the intermetallic layer thickness and the time of annealing at a certain temperature. When the growth of the intermetallic layer occurs only due to the chemical reaction, the value of $n$ is 1, but in the case of volume diffusion, the value of $n$ is 0.5 [8]. In the case when the value of $n$ is in the range between 0.5 and 1 the growth of the intermetallic layer is governed by a mixed mechanism of the chemical reaction and volume diffusion. Growth of the intermetallic layers was mainly in "the direction" of the Al layer, causing its rapid "disappearance" that finally results (after annealing for 10 h) in its complete transformation into intermetallic phases. (Fig. 2c). The growth kinetic calculated in this work is shown in (Fig. 4), and it is compared with the literature data presented in [18,19]. The main differences between the data obtained in this work and the one presented in the literature result from the presence of additional elements in Al or Fe sheets. Based on the literature data, the addition of Si to Al and Zn to Fe results in the formation of much thicker reaction layers than those observed between pure Al and Fe at the same temperature. Furthermore, the ternary $\tau_6$-$Al_{4.5}FeSi$ phase [18], produces another thin layer and makes the bonding region even thicker.

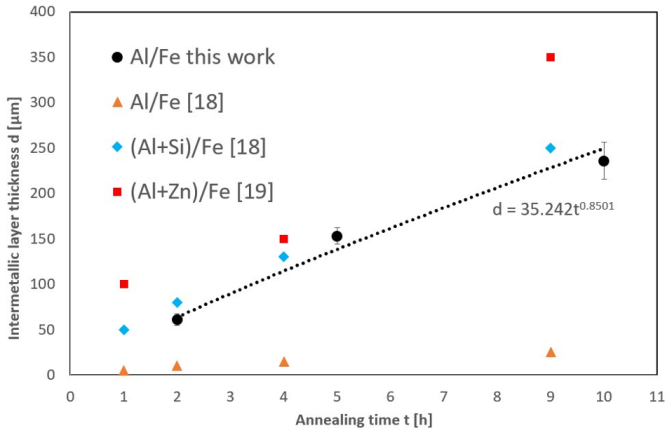


Fig. 4. Effect of annealing time on the average thickness of the intermetallic layer's against the background of the literature data [18,19]

The high-magnification SEM/BSE micrographs revealed the morphology of the intermetallic phases. In areas close to the Al sheet the grains are small (below 10 µm) and nearly equiaxed, whereas in the areas near the Fe sheet the grains are much larger (up to ~60 µm) and elongated (Fig. 3). Similar structures at the interface of the Al/Fe composite fabricated in an air atmosphere were observed by Springer et al. [18].

The chemical composition measurements using STEM/EDS system were conducted in two areas. At first, the point analysis close to the interface between Fe and the intermetallic phase (Fig. 5) revealed the ratio between Al and Fe to be about 71 at. %. and 29 at. % respectively (TABLE 2), which corresponds to the η-$Al_5Fe_2$ phase as the dominant component. The measurements in the thin areas visible at the border of "the fingers" (Fig. 3b) did not reveal any essential chemical composition changes. The X-Ray diffraction patterns from interfacial layers (Fig. 6) and the electron diffraction pattern (Fig. 7) confirmed only the existence of Fe and the η-$Al_5Fe_2$ phase. The STEM/HAADF (Fig. 5) and TEM/bright-field (Fig. 7a) images revealed a formation of elongated grains and small equiaxed grains in this area.The TEM/SAED patterns (Fig. 7b-c) confirmed the different orientations of the η-phase grains of the thin area, compared to the grains inside "the fingers"; this could be the reason for the difference in contrast (channeling) on SEM/BSE images (Fig. 3b).

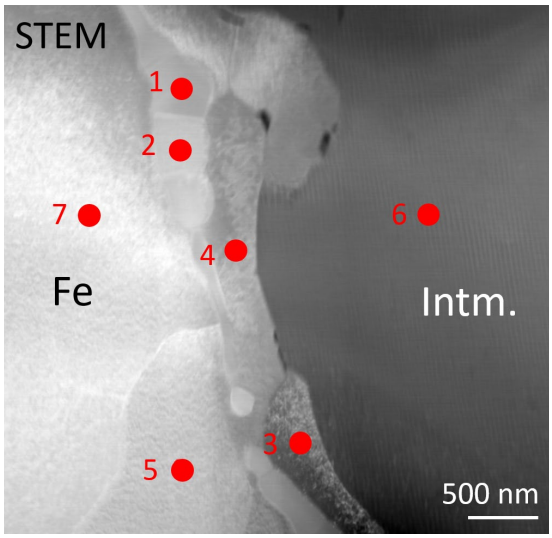


Fig. 5. STEM/HAADF image of the interface between Fe and Intm. with highlighted chemical composition measurement points. The corresponding results were shown in Table 2

TABLE 2

Chemical compositions at points marked in Fig. 5

| Point number | Al (at.%) | Fe (at.%) |
|---|---|---|
| 1 | 70 | 30 |
| 2 | 69 | 31 |
| 3 | 72 | 28 |
| 4 | 72 | 28 |
| 5 | 0 | 100 |
| 6 | 73 | 27 |
| 7 | 0 | 100 |

STEM/EDS point analysis of the intermetallic layer close to the Al-layer revealed a difference in chemical composition between measured points (Fig. 8, TABLE 3). The Al concentration at points 2, 3, and 5 was about 77 at. % while at point 7 did

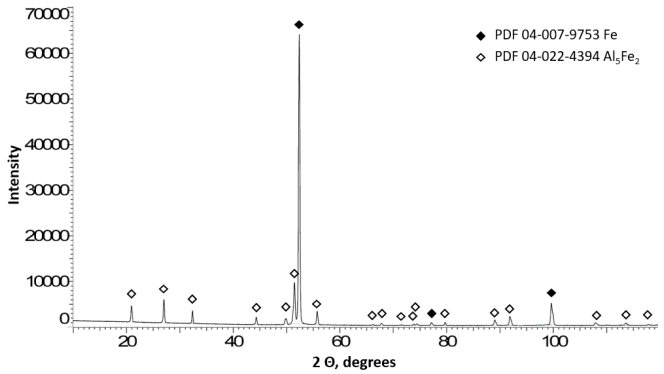


Fig. 6. X-Ray diffraction pattern from the interface between Fe and Al showing $Al_5Fe_2$ intermetallic phase formation

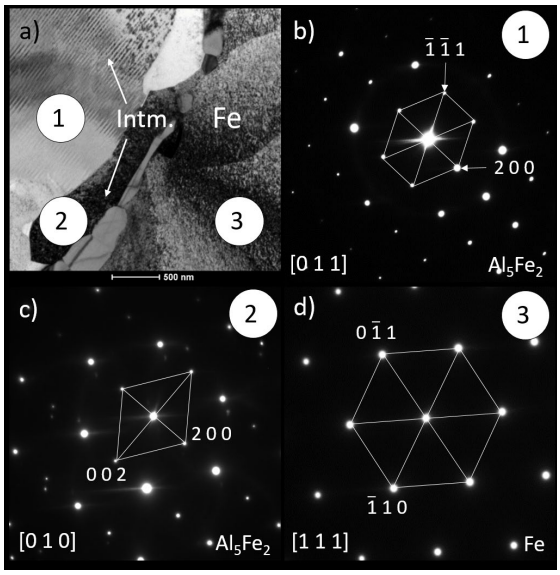


Fig. 7. (a) TEM/bright field image showing the interface between Fe and intermetallic phase and (b-d) corresponding the electron diffraction patterns from areas marked in (a)

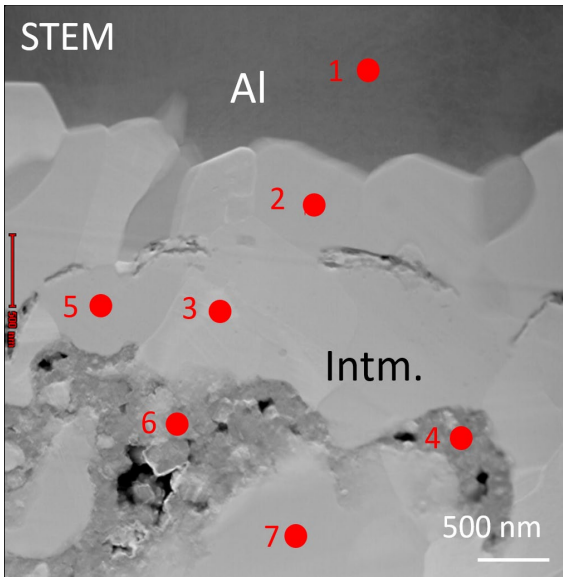


Fig. 8. STEM/HAADF image of the interface between Al and Intm. with highlighted chemical composition measurement points. The corresponding results were shown in Table 3

TABLE 3

Chemical compositions at points marked in Fig. 8

| Point number | Al (at.%) | Fe (at.%) |
|---|---|---|
| 1 | 100 | 0 |
| 2 | 77 | 23 |
| 3 | 76 | 24 |
| 4 | 99 | 1 |
| 5 | 77 | 23 |
| 6 | 99 | 1 |
| 7 | 73 | 27 |

not exceed 73 at. %. The line scan across the intermetallic phase in the sample annealed in 10 h (Fig. 9) also revealed a significant increase of the Al concentration.

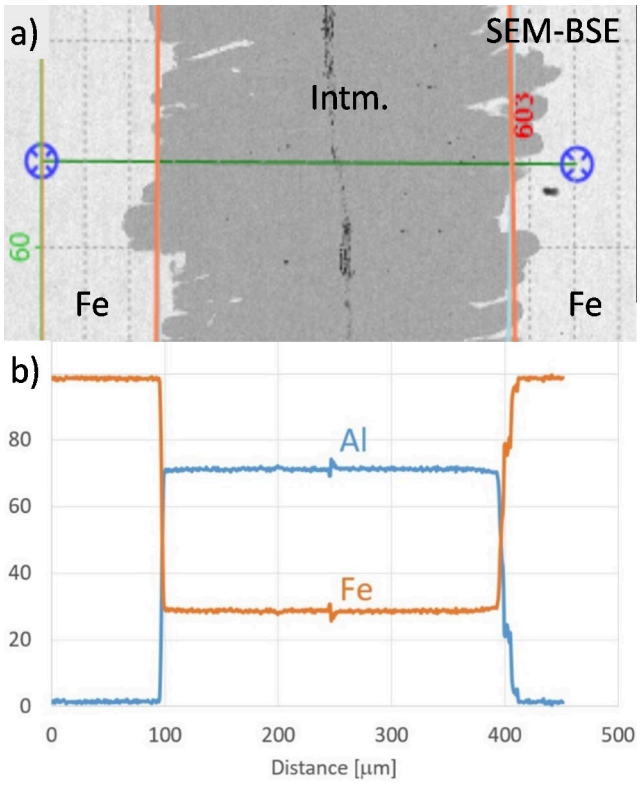


Fig. 9. a) SEM/BSE image showing the intermetallic layer in the sample annealed for 10h and b) SEM/EDS line scan along the green line marked in a)

The TEM examinations of this area revealed a thin "stripe" composed of equiaxed grains (Fig. 10a). The electron diffraction patterns (Fig. 10b-d) are taken from the areas marked as '1' and '2' in Figs. 10b, c show a monoclinic symmetry; this strongly suggests the presence of the θ-$Al_{13}Fe_4$ phase, well-described in the literature [9-10]. The shape of grains of this narrow phase and the electron diffraction patterns vary considerably from the adjacent wide intermetallic phase, which was found to be η-$Al_5Fe_2$ phase (Fig. 10d).

The structure of *θ*-phase is described as a complex structure because of the large unit cell [9]. This complex structure is strongly related to quasicrystals and gives similar (but periodic)

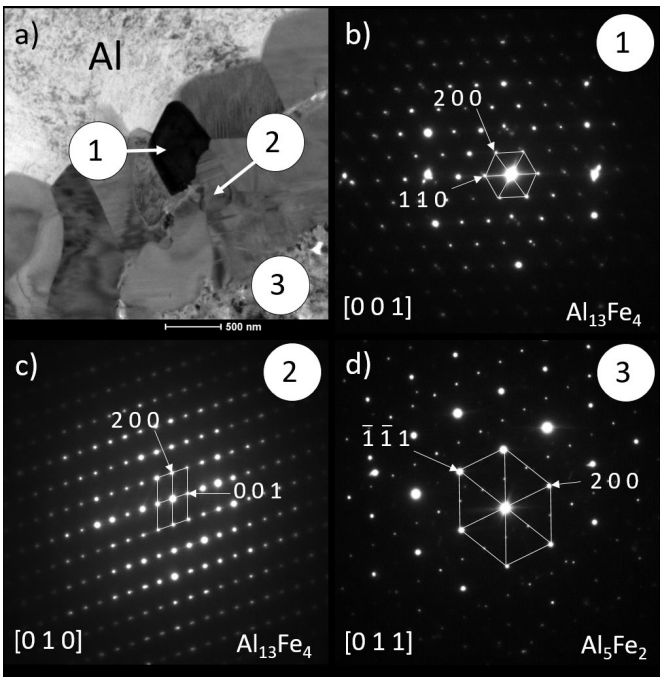


Fig. 10. (a) TEM/bright field image showing the morphology of interface between Al and intermetallic phase and corresponding (b-d) the electron diffraction patterns from areas marked in (a)

X-Ray and TEM/SAED diffraction patterns. The addition of a third element from the group of transition metals (groups 3-12 in the periodic table of elements) could result ininformation of stable quasi-crystalline phase [24].

The full transformation of Al into intermetallic phases after 10 h of hot pressing gives a possibility for further annealing in temperatures higher than the melting temperature of Al, thus it is possible to produce the composites with more intermetallic phases like AlFe and $Al_2Fe$.

### 3.2. Microhardness measurements

The microhardness measurements were conductednear the 18th interface along with the intermetallic layer and also in Fe and Al sheets for comparisonof the sample annealed for 5 hours. The average microhardness value for the η-$Al_5Fe_2$ phase is about 780 HV, which makes it one of the hardest phases occurring in metal alloys. However, some cracks appear in the intermetallic layer during indentation, which confirms its high brittleness (Fig. 11). The average microhardness values for Fe and Al are about 99 HV and 20 HV, respectively (Fig. 12, TABLE 4). The total volume of the intermetallic layer increases with the annealing time and finally, after 10 hours their volume fraction reaches the value of 52% (Fig. 13a). Thus, the 'average' hardness of the composite, estimated by multiplying the hardness value of the component by its volume fraction, is the highest (Fig. 13b).

TABLE 4

'Average' microhardness. of layers. $\rho$ is the standard deviation $\pm$

| Phase | μHV | $\rho$ |
|---|---|---|
| Al | 20 | 1 |
| Fe | 100 | 3 |
| Intm ($Al_5Fe_2$) | 780 | 9 |

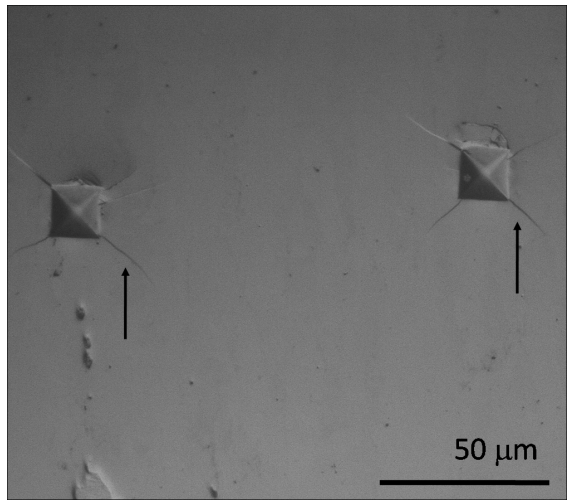


Fig. 11. The optical microscopic image of the intermetallic layer after indentation

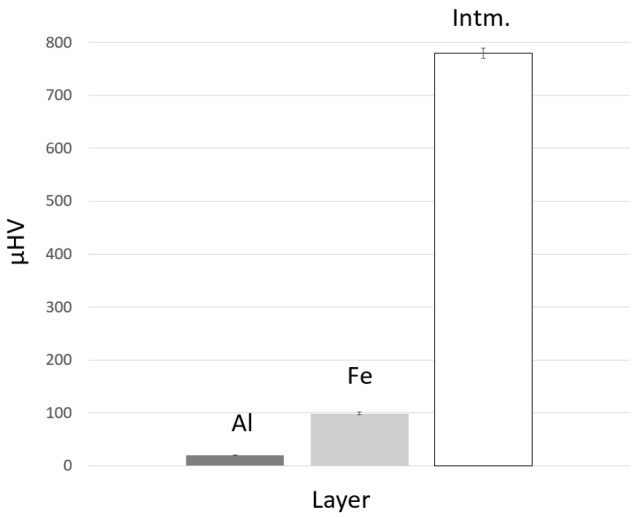


Fig. 12. Microhardness of particular component of the composite

### 4. Conclusions

The hot pressing under an air atmosphere shows to be an interesting alternative as compared to other methods used for producing MIL composites with attractive mechanical properties. Using this method, it is possible to reduce the costs of manufacturing because it does not need a complicated and expensive vacuum or inert gas installations.

In Al/Fe system, the intermetallic phase forms just after 2 hours of annealing at 903 K under the pressure of 30 MPa. Increasing the time of annealing results in the growth of the reaction layer's thickness and finally after 10 hours, the Al layer completely transforms into intermetallic phases. The total volume of the intermetallic layer reaches a value above 50% of the

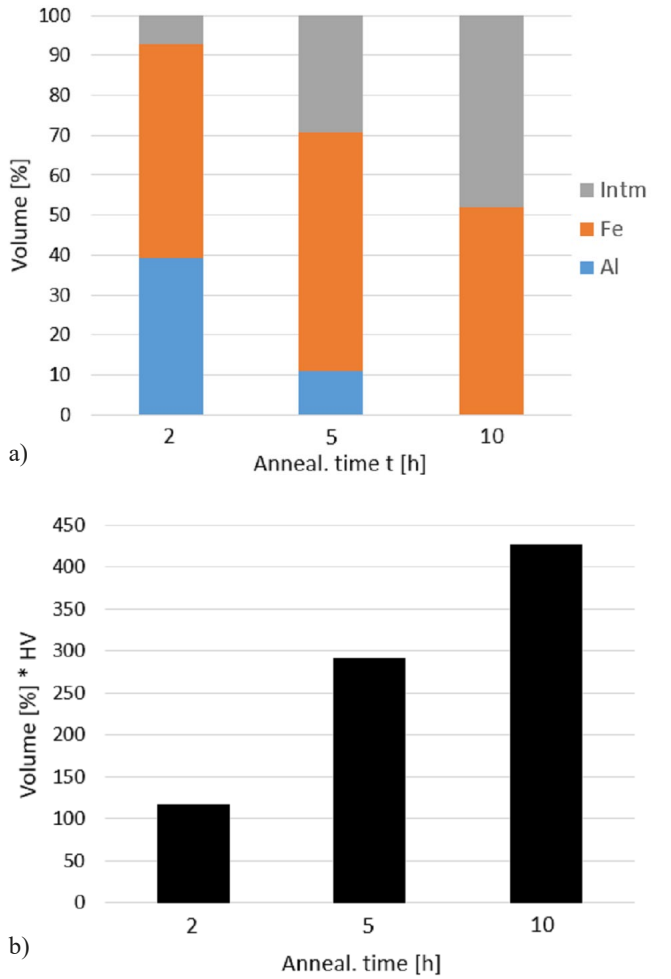


Fig. 13. (a) Volume fraction of individual composite components and (b) 'averaged' composite microhardness including volume fraction of individual components

sample volume. Two intermetallic phases have been confirmed, i.e. $Al_5Fe_2$ with orthorhombic symmetry and $Al_{13}Fe_4$ with monoclinic symmetry and complex structure.

Microhardness measurements showed a very high hardness of the layers composed of intermetallic phases, which is close to 780 HV. Using hot pressing of Al and Fe at 903 K for 10 h it is possible to obtain composites with very high hardness and stiffness.

The complete transformation of Al into intermetallic phases gives the possibility for further heat treatment of these composites at a temperature higher than the melting temperature of Al. The present intermetallic phases, which are very hard but also brittle, could react with Fe and produce other phases like AlFe and $Al_2Fe$; thus it is possible to produce MIL composites with better mechanical properties.

**Acknowledgements**

The work was supported by The National Centre for Research and Development (NCBiR) in the frame of TECHMATSTRATEG2/412341/8/NCBR/2019 (EMuLiReMat).

## REFERENCES

[1] M. Krasnowski, T. Kulik, Nanocrystalline and amorphous Al-Fe alloys containing 60-85% of Al synthesised by mechanical alloying and phase transformations induced by heating of milling products, Mater Chem. Phys. **116**, 631-637 (2009). DOI: https://doi.org/10.1016/j.matchemphys.2009.05.003

[2] M. Krasnowski, T. Kulik, Nanocrystalline Al-Fe intermetallics – lightweightalloys with high hardness, Intermetallics **18**, 47-50 (2010). DOI: https://doi.org/10.1016/j.intermet.2009.06.006

[3] X. Li, A. Scherf, M. Heilmaier, F. Stein, The Al-rich part of the Fe-Al phase diagram, J. PhaseEqulib. Diff. **37**, 162-173 (2016). DOI: https://doi.org/10.1007/s11669-015-0446-7

[4] G.H.S.F.L. Carvalho, I. Galvão, R. Mendes, R.M. Leal, A. Loureiro, Explosive welding of aluminium to stainless steel, J. Mater. Process. Tech. **262**, 340-349 (2018). DOI: https://doi.org/10.1016/j.jmatprotec.2018.06.042

[5] G.H.S.F.L. Carvalho, I. Galvão, R. Mendes, R.M. Leal, A. Loureiro, Formation of intermetallic structures at the interface of steel-to-aluminium explosive welds, Mater. Charact. **142**, 432-442 (2018). DOI: https://doi.org/10.1016/j.matchar.2018.06.005

[6] Z. Guo, M. Liu, Z. Bian, M. Liu, J. Li, An Al-7Si alloy/cast iron bimetallic composite with super-high shear strength, J. Mater. Res. Tech. **8** (3), 3126-3136 (2019). DOI: https://doi.org/10.1016/j.jmrt.2017.06.014

[7] H. Paul, Ł. Maj, M. Prażmowski, A. Gałka, M. Miszczyk, P. Petrzak, Microstructure and mechanical properties of multilayered Al/Ti composites produced by explosivewelding, Procedia Manufacturing **15**, 1391-1398 (2018). DOI: https://doi.org/10.1016/j.promfg.2018.07.343

[8] D.M. Fronczek, R. Chulist, Z. Szulc, J. Wojewoda-Budka, Growth kinetics of $TiAl_3$ phase in annealed Al/Ti/Al explosively welded clads, Mater. Lett. **198**, 160-163 (2017). DOI: https://doi.org/10.1016/j.matlet.2017.04.025

[9] Y. Liu, X. Chong, Y. Jiang, R. Zhou, J. Feng, Mechanical properties and electronic structures of Fe-Al intermetallic, Physica B **506**, 1-11 (2017). DOI: http://dx.doi.org/10.1016/j.physb.2016.10.032

[10] M.Z. Khalid, J. Friis, P.H. Ninive, K. Marthinsen, A. Strandlie, Ab-initio study of atomic structure and mechanical behaviour of Al/Fe intermetallic interfaces, Comput. Mater. Sci. **174**, 109481 (2020). DOI: https://doi.org/10.1016/j.commatsci.2019.109481

[11] N.L. Okamoto, J. Okumura, M. Higashi, H. Inui, Crystal structure of η'-$Fe_3Al_8$; low-temperature phase of η-$Fe_2Al_5$ accompanied by anordered arrangement of Al atoms of full occupancy in the c-axis chain sites, Acta Mater. **129**, 290-299 (2017). DOI: http://dx.doi.org/10.1016/j.actamat.2017.02.060

[12] H. Springer, A. Kostka, J.F. dos Santos, D. Raabe, Influence of intermetallic phases and Kirkendall-porosity on the mechanical properties of joints between steel and aluminium alloys, Mat. Sci. Eng A **528**, 4630-4642 (2011). DOI: https://doi.org/10.1016/j.msea.2011.02.057

[13] P. Clérico, X. Mininger, L. Prévond, T. Baudin, A.L. Helbert, Compromise between magnetic shielding and mechanical strength of thin Al/Steel/Al sandwiches produced by cold roll bonding:

Experimental and numerical approaches, J. Alloys Comp. **798**, 67-81 (2019). DOI: https://doi.org/10.1016/j.jallcom.2019.05.243

[14] F. Kong, Y. Chen, D. Zhang, Interfacial microstructure and shear strength of Ti-6Al-4V/TiAl laminate composite sheet fabricated by hot packed rolling, Mater. Design **32**, 3167-3172 (2011). DOI: https://doi.org/10.1016/j.matdes.2011.02.052

[15] H. Xiao, Z. Qi, C. Yu, C. Xu, Preparation and properties for Ti/Al clad plater generated by differential temperature rolling, J. Mater. Process. Tech. **249**, 285-290 (2017). DOI: https://doi.org/10.1016/j.jmatprotec.2017.06.013

[16] M. Yang, H. Ma, Z. Shen, D. Chen, Y. Deng, Microstructure and mechanical properties of Al-Fe meshing bonding interfaces manufactured by explosive welding, Trans. Nonferrous Met. Soc. China **29**, 680-691 (2019). DOI: https://doi.org/10.1016/S1003-6326(19)64978-2

[17] M. Fan, Z. Luo, Z. Fu, X. Guo, J. Tao, Vacuum hot pressing and fatigue behaviors of Ti/Al laminate composites, Vacuum **154**, 101-109 (2018). DOI: https://doi.org/10.1016/j.vacuum.2018.04.047

[18] H. Springer, A. Kostka, E.J. Payton, D. Raabe, A. Kaysser-Pyzalla, G. Eggler, On the formation and growth of intermetallic phases during interdiffusion between low-carbon steel and aluminium alloys, Acta Mater. **59**, 1586-1600 (2011). DOI: https://doi.org/10.1016/j.actamat.2010.11.023

[19] H. Springer, A. Szczepaniak, D. Raabe, On the role of zinc on the formation and growth of intermetallic phases during interdiffusion between steel and aluminium alloys, Acta Mater. **96**, 203-211 (2015). DOI: https://doi.org/10.1016/j.actamat.2015.06.028

[20] J. Yang, Y.L. Li, H. Zhang, W. Guo, Y. Zhou, Control of interfacial intermetallic compounds in Fe-Al joining by Zn addition, Mat. Sci. Eng. A **645**, 323-327 (2015). DOI: https://doi.org/10.1016/j.msea.2015.08.036

[21] C. Tan, C. Zang, H. Xia, X. Zhao, K. Zhang, S. Meng, B. Chen, X. Song, L. Li, Influence of Al additions in Zn-based filler metals on laser welding-brazing of Al/steel, J. Manuf. Process. **34**, 251-263 (2018). DOI: https://doi.org/10.1016/j.jmapro.2018.06.008

[22] W. Kowalski, H. Paul, P. Petrzak, Ł. Maj, I. Mania, M. Faryna, Influence of hot pressing on the microstructure of multi-layered Ti/Al composites, Arch. Metall. Mater. **66** 4, 1149-1156 (2021). DOI: https://doi.org/10.24425/amm.2021.136435

[23] W. Gąsior, A. Debski, Z. Moser, Formation enthalpy of intermetallic phases from Al-Fe system measured with solution calorimetric method, Intermetallics **24**, 99-105 (2012). DOI: https://doi.org/10.1016/j.intermet.2012.02.001

[24] R.T. Li, Z.L. Dong, K.A. Khor, Al-Cr-Fe quasicrystals as novel reinforcements in Ti based composites consolidated using high pressure spark plasma sintering, Mater. Design **102**, 255-263 (2016). DOI: https://doi.org/10.1016/j.matdes.2016.04.040